Transp Porous Med (2009) 80:1–16
DOI 10.1007/s11242-009-9340-2

Experimental Study of Upward Oil Migration in a Fracture

Didier Loggia · Zhou Bo · Luo Xiaorong · Guy Vasseur

Received: 4 September 2008 / Accepted: 11 January 2009 / Published online: 7 February 2009

Abstract The upward oil migration in a transparent and rough fracture containing a liquid of higher density is studied experimentally using a light transmission technique. The aperture heterogeneity is also measured by light transmission. The injection of oil in a fracture containing a heavier fluid produces a gravitational fingering instability. Depending on the injection velocity (capillary number, Ca) and the density difference between the two fluids (Bond number, Bo), different patterns are observed during the oil displacements. The width of the finger and its velocity are measured as a function of Bo and Ca. A stability analysis of the interface, based on a generalised Darcy equation in a two-dimensional fracture, allows an accurate description of the experimental results. The order of magnitude of the finger width and its velocity are in good agreement with the calculations, with small disparities due to various unknown fluid flow parameters: capillary pressure, finger thickness in the gap of the fracture, finger tortuosity and oil velocity field into the finger. The theoretical approach allows constructing a (Ca, Bo) phase diagram of stability of the interface.

Keywords Percolation · Buoyancy · Capillary flow · Viscous · Fracture · Heterogeneity

1 Introduction

Immiscible fluid flow in fracture is an active field of research due to its large number of applications, e.g. in the areas of petroleum geology and hydrology. In particular, the model-

D. Loggia (✉)
Laboratoire Géosciences Montpellier, Université Montpellier 2, INSU-CNRS, Place E. Bataillon, 34095 Montpellier cedex 5, France
e-mail: loggia@univ-montp2.fr

Z. Bo · L. Xiaorong
Key Laboratory of Mineral Resource, Institute of Geology and Geophysics, Chinese Academy of Sciences, Beijing 100029, China

G. Vasseur
SISYPHE, UMR 7619, Boîte 123, Université Paris 6, 75252 Paris cedex 5, France

ling of oil secondary migration or Dense Non-Aqueous Phase Liquid (DNAPL) infiltration in a fracture is a major challenge, due to the presence of fingering instabilities, and due to the complex multi-scale heterogeneity of a fracture. The dynamics of fingering between the wetting and non-wetting fluids in the fracture is governed by the interplay among capillary, viscous and gravity forces. These forces can act simultaneously, and have important implications in the determination of the fingering pattern and its velocity. Their relative importance is classically characterised by two dimensionless numbers, the capillary number (Ca) and the Bond number (Bo), which are defined in the discussion paragraph.

The upward oil percolation was mainly studied in porous media, and two principal theoretical approaches have been employed. The first approach concerns very low velocity quasistatic displacement: the oil invades a random lattice of throats with a step by step procedure, and the displacement pattern is dominated by the growth of a single branch (Wilkinson 1984). In this gravity destabilised percolation process, a power law relating the width of the branch and the density difference (via the Bond number) was emphasised. More recently, it was shown that the width of the branch is controlled by both the density difference and the width of the capillary pressure distribution (Bo et al. 2006). The second approach is dynamic and makes use of the continuum mechanics equation, where a macroscopically defined fluid flow velocity is related to the fluid pressure gradient (Darcy law) and to the capillary pressure (Catalan et al. 1992). These equations were successfully used in the past (Chuoke et al. 1959; Peters and Flock 1981) to describe the width of viscous and/or gravitational fingers in porous media. Several studies attempted to improve a better quantitative description of the finger width selection in porous media (Riaz and Tchelepi 2004, and references therein). More recently, a new model, also based on the macroscopic Darcy equation was proposed to estimate the (DNAPL) velocity of a conceptual mobile-immobile-zone finger model in porous media (Zhang and Smith 2001). Besides the percolation model and the continuum mechanics models, there exist different approaches, such as Monte Carlo simulation, stochastic aggregation model or modification of the invasion percolation model (Ewing and Berkowitz 1998; Glass and Yarrington 1996).

However, much less attention has been dedicated to immiscible displacements in fractures. The reference work of Saffman and Taylor (1958) concerns the phenomena of viscous and/or gravitational fingering in a Hele Shaw cell. These authors performed a linear analysis, predicting the stability of the interface. This allows defining the conditions required to get fingering and to investigate the length scale of the fingers. A slight modification of the calculation of the capillary pressure was performed (Park et al. 1984), giving a better agreement with the width of the fingers. Recent studies have shown that a quantitative analysis of fingering in a heterogeneous fracture is confronted to an indetermination of the capillary pressure. Glass et al. (1998) have shown that, in a fracture, the capillary pressure depends on two radii of curvature. The first one is the curvature radius of the fluid interface in the plane of the fracture. The second one is defined perpendicularly to the plane of the fracture, its order of magnitude being given by the aperture of the fracture. Various authors (DiCarlo and Blunt 2000; Nicholl and Glass 2005) have used the concept of dynamic capillary pressure to obtain a better description of the finger shape and the finger width. In most of the studies concerning Hele Shaw cell, it is assumed that the capillary pressure depends, at the first order, on the curvature radius in the plane of the fracture, the perpendicular curvature radius being unimportant (Bensimon et al. 1986; Zhang et al. 1998). Indeed, a recent numerical study Glass et al. (1998) suggests that this assumption is valid in a Hele Shaw cell, where the correlation length of the aperture (which is infinite in a Hele Shaw cell) is much larger than the aperture. On the contrary, in a heterogeneous and particularly rough fracture, the correlation length of the aperture can sometimes be finite and much smaller than the mean aperture. In this case,

it was shown that the capillary pressure is mainly controlled by the aperture, leading to an invasion percolation process (Glass et al. 1998; Amundsen et al. 1999). Several experiments were performed (Nicholl et al. 1994) to study the downward water infiltration through dried or partially dried fracture. The finger widths were studied as a function of the injection flow rate (and the finger velocity), while the finger velocity was studied as a function of the finger length. A good theoretical description of the fingers was obtained when using the assumptions that the capillary pressure depends on the radius curvature in the plane of the fracture, and that the capillary pressure is velocity dependant.

To our knowledge, there are very few quantitative experimental studies of the different instability fingering patterns for upward oil displacement in fracture. Most of the studies concern water–air density driven flows (Nicholl and Glass 2005; Amundsen et al. 1999). In the present paper, we study experimentally the upward vertical invasion of oil in a fracture where the fluid initially in place is a wetting fluid of higher density. Similar to what occurs for the downward water infiltration in a fracture containing air, upward oil migration in a fracture containing water produces a gravitational instability and fingering. In the first part of the paper, we present the aperture field measurement of the fracture. The second part illustrates qualitatively the oil pattern during the migration and at the percolation threshold. In the third part, a discussion is presented concerning the finger width and the finger velocity, as a function of the injection velocity and the density difference between the oil and the defending fluid. Results are compared to available theoretical models of fingering instability.

2 Experiments

A schematic illustration of the experiment is given in Fig. 1. Two glass plates with a rough surface are obtained from industrial decorative material called 'cathedral glass'. In the plane

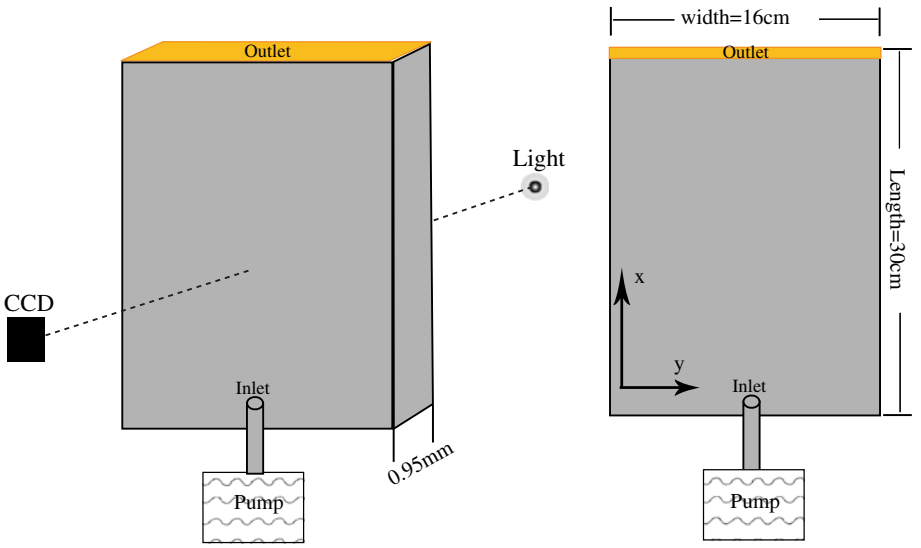

(a) side view **(b)** planform

Fig. 1 Sketches of our experiment in plan and cross-sectional views. The fracture, the injection pump, the CCD camera and the lighting system. The x axis is parallel to the oil displacement direction

(xy) of the fracture, the two glass plates have a length $L = 30$ cm along the flow direction (x), and a width $l = 16$ cm in the transverse direction (y). The thickness of the glass plates is 3 mm. A special care is achieved for assembling the two faces with a constant mean aperture. In order to obtain a perfect parallelism between the glass plates (and then a constant mean aperture inside the fracture), long cylindrical metallic wedges are placed at fixed locations around the fracture. The sides and the bottom of the glass plates are made impervious with a rubber ring surrounding the fracture. At the bottom of the cell, the oil can be injected with a double syringe pump (Pharmacia P500) at a controlled flow rate; the fluid enters through the fracture via a nozzle of inner diameter 1 mm. At the top of the cell, the liquid is evacuated along the whole width of the fracture, and conducted through an overflow. The fracture position is always vertical, and so the fluid displacement is made against the gravity direction.

The injected fluid always remains the same, a dibutyl-phthalate (an oil of specific weight $\rho_o = 1.043$ g/cm^3, viscosity $\mu_o = 21$ cP and interfacial tension $\gamma = 13.0$ dyn/cm). The oil is dyed with a red organic dye, added in concentration 0.05 g/l. In order to analyse the effect of the flow velocity, this oil is injected with three different flow rates $Q = 5, 25,$ or 100 cm^3/h. The non-miscible displaced fluid is a degassed and deionised water–sucrose mixture solution (WSMS). In order to study the effect of density difference between the oil and the WSMS, four WSMS are selected, with massic concentrations of sucrose $c_S = 15\%, 20\%, 25\%$ and 35%. The sucrose concentration increases the specific weight ρ_w of the WSMS (which for the cited values of c_S respectively are 1.054, 1.0752, 1.0996 and 1.1445 g/cm^3), and increases slightly its viscosity μ_w (which are respectively 1.6, 1.96, 2.4 and 4 cP). During the oil displacement, the oil saturation is recorded by a (12-bit) CCD camera, which furnishes pictures of 900×470 pixels (the pixel size is 0.34 mm) at regular time intervals, until the oil reaches the top of the column (at the percolation threshold). The lighting system is made of led light with a constant supply voltage. It is placed far behind the fracture, in front of the camera. It provides a constant light and allows to clearly delineate the interface between oil and WSMS in the picture.

After the oil displacement, the faces of the fracture and the ring are completely disassembled, and the whole system is submitted to several bathing and rinsing using acetone, ethanol and distilled water. Using this procedure, we have checked that we obtain a water wet surface and reproducible experiments.

3 Results

3.1 Mean Aperture and Aperture Field Measurements

In order to measure the mean aperture of the fracture, we use a simple flow configuration experiment where the fluid velocity can be related to the mean aperture field. In the first step, the cell is filled with air, and we inject from the bottom a degassed and deionised distilled water at a constant volumetric flow rate Q. At high enough flow rate, we always observe a stable and flat water–air interface, moving upward with a constant velocity q. This is a consequence of the viscous-gravitational stabilisation of the front (in this displacement, the more viscous fluid displaces the less viscous one, and the denser fluid stays below the lighter), which hides the heterogeneity; therefore, no preferential path flow is observed in this configuration. The mean fracture aperture $\bar{b}$ is obtained from the relation giving the mean velocity of the horizontal water–air interface, $(q = Q/(l\bar{b}))$. In order to obtain a better precision in the aperture measurement, experiments are performed at different flow rates, allowing to determine the mean aperture of the fracture, $\bar{b} = 0.95$ mm. Note that the technique used

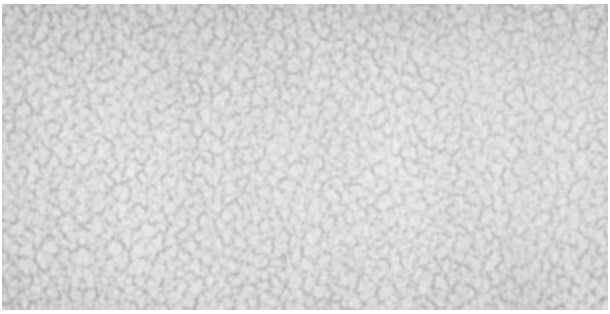

Fig. 2 Gray scale picture of the aperture of the fracture, measured with a transmission light method. The fracture length is $L = 30$ cm, width is $l = 16$ cm, the mean value of the aperture is 0.95 mm and the pixel size is 0.34 mm

here to obtain the mean aperture is quite similar to the technique presented in a previous study (Detwiler et al. 1999), except that, here, we have slightly modified and simplified the procedure through the use of a piston-like displacement.

In the second step, the aperture field is precisely measured using a classical transmission light technique. The technique was previously described in detail (Detwiler et al. 1999); we just recall here the basic principle. It consists of successively measuring the intensity of transmitted light $I^1_{i,j}$ through the fracture filled with dyed water (filtered blue methyl dyed water with a dye concentration $c_1 = 0.05$ g/l), and the intensity of transmitted light $I^2_{i,j}$ through the fracture filled with distilled water (the dye concentration is then $c_2 = 0$). Taking the average of $I_{i,j}$ over the whole cell, the application of the Beer-Lambert law ($I_{i,j} = I_0 \exp(-\mu b_{i,j} c)$, where I_0 is the incident light intensity, μ is the light attenuation coefficient and c is the dye concentration) leads to the determination of the local aperture $b_{i,j} = \bar{b}\ \ln(I^1_{i,j}/I^2_{i,j})/\langle \ln(I^1_{i,j}/I^2_{i,j})\rangle$.

The aperture obtained is depicted in Fig. 2. A histogram analysis shows that the aperture is practically Gaussian and ranges between 0.49 and 1.17 mm, with a mean value of 0.95 mm. This is not a perfect Hele Shaw cell, but there is no strong closing or opening of the aperture field; the aperture fluctuates smoothly around its mean value. The spatial correlation of the aperture is studied by calculating autocorrelation functions (Loggia et al. 2004), which are estimated along the longitudinal and transverse direction to the displacement. This spatial correlation function displays a fast exponential decay on a length less than 5 mm; this decay is always found independent on the direction calculation. It means that the spatial aperture is spatially isotropic and correlated with a correlation length $\lambda = 5$ mm. This correlation length is small compared to the size of the fracture ($L \times l \approx 60\lambda \times 32\lambda$), and so large scale heterogeneities are not present.

Moreover, the order of magnitude of λ and $\bar{b}$ are nearly similar. According to recent numerical simulations of immiscible displacement (Glass et al. 1998), the capillary forces may be controlled by both curvature radii: in the plane of the fracture and in a plane perpendicular to the fracture.

3.2 Time Evolution Pattern

Typical time evolution pattern of the oil saturation is given for three particular viscous-density contrasts in Fig. 3. Pictures are obtained at regular time intervals with time increasing from the left to the right picture.

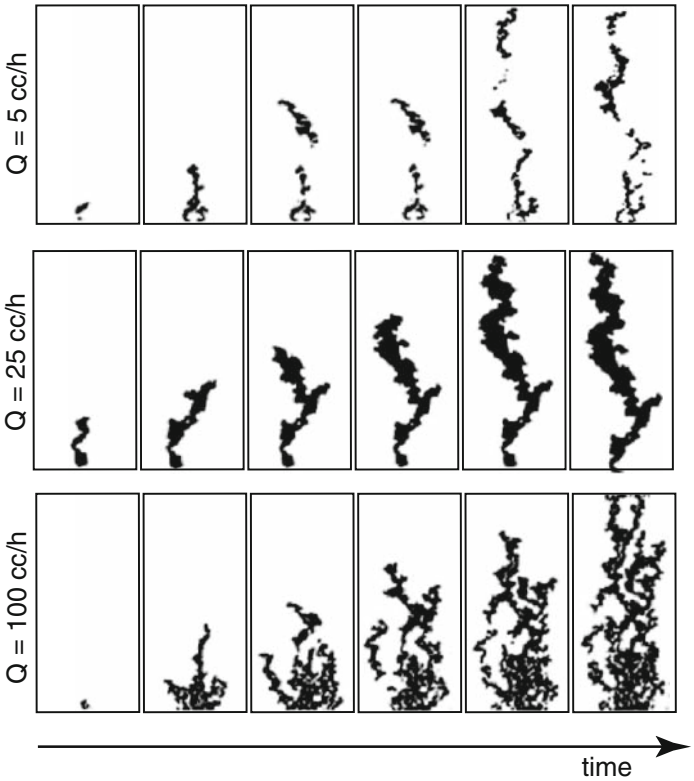

Fig. 3 CCD picture of oil (in black) displacing a water sucrose mixture (in white). The oil is injected from the bottom of the transparent fracture at different flow rates ($Q = 100\,\mathrm{cm}^3/\mathrm{h}$, $25\,\mathrm{cm}^3/\mathrm{h}$, $5\,\mathrm{cm}^3/\mathrm{h}$, respectively, from the bottom to the top). The time interval between each picture is not the same for the three experiments; it is respectively 90 s, 320 s and 480 s. Pictures are made binary using a threshold algorithm

In the 6 pictures on the bottom, the injection flow rate is $Q = 100\,\mathrm{cm}^3/\mathrm{h}$, and the displaced fluid is the denser one, a WSMS with a sucrose concentration of 35%. Pictures are displayed every 90 s. Three fingers appear in the beginning of the invasion experiment, but these fingers rapidly merge. In the following, this gives rise to a complex pattern made of randomly growing clusters and fingers. We note the presence of trapping phenomenon where a considerable non-invaded zone filled with the WSMS remains surrounded by the oil. Despite the high mean velocity displacement ($\sim 65\,\mathrm{cm/h}$), no stable piston-like front is observed. Viscous effects are too small to totally stabilise the interface. It is difficult to define whether the finger growth is due to gravitational forces or/and capillary preferential flow path, but the resulting pattern is a tortuous cluster with many fingers.

For the 6 pictures in the middle of Fig. 3, the flow rate is lower, $Q = 25\,\mathrm{cm}^3/\mathrm{h}$, and a lighter WSMS is displaced ($c_S = 20\%$). Pictures are displayed every 320 s. The oil pattern presents a single and tortuous gravitational finger. The mean tip velocity of the finger is estimated at 0.15 mm/s; this value is 15 times greater than the mean injection velocity $Q/\bar{b}l$, which is nearly 0.01 mm/s. The high density difference between the initial fluid in place and the injected fluid produces an important gravitational instability, which results in a single finger growing up with high velocity. The large tortuosity of the finger indicates that this preferential flow path is due to capillary forces acting on the displacement. The absence

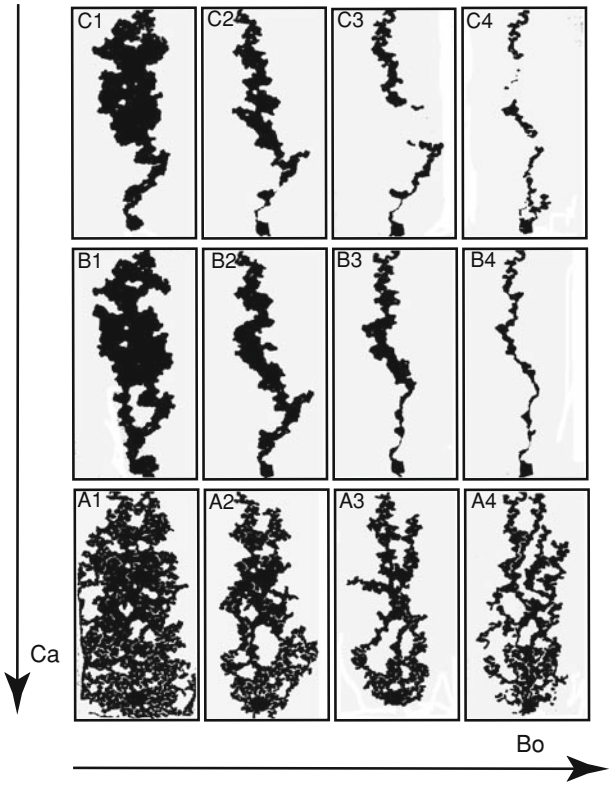

Fig. 4 Oil (black) displacing water sucrose mixture (white) at different Bond numbers and capillary numbers. For each experiment, the pictures represent the oil pattern at the percolation threshold. We observe 4 different regimes: piston-like displacement with trapping (A1), random clusters with numerous tortuous fingers (A2, A3, A4), single and tortuous finger (B2, B3, C1, C2) and single and tortuous finger with fragmentation (B4, C3, C4)

of flattening for the oil-WSMS interface indicates that viscous forces are negligible. The resulting pattern is a single and tortuous gravitational finger.

On the top of Fig. 3, the flow rate is the lowest, $Q = 5\,\mathrm{cm}^3/\mathrm{h}$, and the displaced WSMS is the heaviest ($c_S = 35\%$). Pictures are displayed every 480 s. The results here are nearly similar to the previous one at $25\,\mathrm{cm}^3/\mathrm{h}$, with the growth of a tortuous finger at a very high tip velocity. Comparing with the previous experiment, the growing finger appears thinner and less tortuous. Moreover, the high density contrast here allows snap-off events which produce migration of disconnected fragments of the non-wetting fluid.

3.3 Final Pattern at the Percolation Threshold

In the previous section, it was possible to visualize the effect of gravitational fingering, capillary fingering and viscous stabilisation. In the present section, we present the whole spectrum of possible oil patterns due to these forces. The oil pattern is depicted in Fig. 4, at the percolation threshold (when the oil reaches the top of the cell), for 4 particular viscous-density contrasts, and 3 different flow rates. Depending on the flow rate and the viscous-density contrast, the observed phenomena can be divided into 4 distinct regimes, as described in the following :

– piston like displacement with trapping: At high velocity and with a low density contrast (picture A1), we observe an interface practically flat which invades the fracture with a constant velocity. This interface is stabilised by viscous forces and/or capillary forces, which are known to increase with the velocity (DiCarlo and Blunt 2000). Due to capillary effects or/and preferential flow path in zones of higher aperture, we observe a partial trapping of the wetting phase. The resulting pattern at the percolation threshold gives random oil clusters located inside the whole cell, with few zones of trapping where the defending phase remains immobile.
– random clusters with numerous tortuous fingers: At high velocity but with a higher density contrast (pictures A2, A3, A4), the destabilising density effect is more important, and the viscous and capillary stabilisation effects are reduced. Several fingers grow randomly through the heterogeneous structure, enhanced by the gravity and certainly following the zone of higher aperture, where the capillary resistance is minimum. Capillary and/or gravitational fingering are then predominant.
– single and tortuous finger: At lower velocity and with a significant high density contrast (pictures B2, B3, C1, C2), the stabilisation forces (viscous and capillar ones, which flatten the interface) vanish totally. The gravitational fingering effect becomes predominant, and a single finger evolves vertically. However, the evolution of the finger is tortuous; the trajectory is controlled by the heterogeneity of the aperture and/or capillary effect. In this regime, isolated clusters and trapping phenomena are not present.
– single and tortuous finger with fragmentation: At very high density contrast and with a low flow velocity (pictures B4, C3, C4), the regime of displacement is similar to the previous one. However, gravitational effects are reinforced, allowing the presence of fragmentation (snap-off events).

4 Discussion

4.1 Dimensionless Number

In this chapter, we propose to quantitatively analyse the width of the finger and its velocity, as a function of flow velocity and density difference between the oil and the defending fluid. For a quantitative description of the oil–water displacement, we use two classical dimensionless numbers. The first one is the Bond number, $Bo = \frac{(\rho_w - \rho_o) g \bar{b}^2}{\gamma}$, which is the ratio between gravitational and capillary pressure jump. The pressure jumps are estimated at a length scale equal to the mean aperture of the fracture. The second one is the capillary number, which is the ratio between the viscous pressure and capillary pressure jump at the same length scale. It reads $Ca = \frac{\mu_o q \bar{b}^2}{\gamma k}$. It depends on the permeability k of the fracture. In our case, for a smooth fracture with a low degree of heterogeneity, the permeability of a fracture of mean aperture $\bar{b}$ is at the first order $k = \bar{b}^2/12$ (Nicholl et al. 2000). Therefore, the capillary number can be simplified, and reads $Ca = \frac{12 \mu_o q}{\gamma}$.

4.2 Instability Velocity Threshold

When a lighter and more viscous fluid is injected from bottom to top, to displace a denser and less viscous fluid, two situations have to be distinguished. At low velocity, viscous forces are negligible, and the gravitational forces which destabilise the interface are predominant: the resulting flow is then dominated by the instability leading to gravitational fingering. At very high velocity, gravitational forces vanish, and the viscous effects act as a stabilising force,

leading to a stable and nearly planar oil–water interface (piston like displacement). Thus, the flow is unstable at low velocity, and stable at high velocity. There exists a critical velocity q_c above which the flow is stable: this critical velocity is well known (Loggia et al. 1995) and was calculated by Saffman and Taylor (1958) for fluid flow in a Hele Shaw cell. It reads $q_c = -kg\frac{\rho_o-\rho_w}{\mu_o-\mu_w}$. We verify that all our experiments are performed at an injection velocity lower than q_c; as can be noted in Figs. 3 and 4, all the displacement patterns are unstable. After some straightforward calculations, it is easy to show that the ratio between the flow velocity and the critical velocity can be written as a function of the two dimensionless numbers Ca' and Bo:

$$\frac{Ca'}{Bo} = \frac{q}{q_c} \tag{1}$$

where $Ca' == \frac{12(\mu_o-\mu_w)q}{\gamma}$ is a modified capillary number that takes into account the water and oil viscosities. Equation 1 will be useful in the following sub sections.

4.3 Finger Width

In the first approach, we plot in log-log coordinates the mean width W of the finger versus the Bond number. For the lowest velocity displacement ($Ca = 1.77E-4$ and $Ca = 8.87E-4$), we observe a power law relating these two parameters, written as $W \sim Bo^{-0.64}$. This result can be compared to that obtained for destabilized invasion percolation in porous media (Wilkinson 1984; Bo et al. 2006): a similar power law is obtained. However, in porous media, the theory of Invasion Percolation in a Gradient (IPG) cannot be strictly applied to oil displacement through a fracture (the capillary pressure is different in porous media and in fractures, and IPG is a quasistatic process in opposition to our experiments).

In order to interpret the finger width dependance with the Bond number, it is more appropriate to make use of classical continuum fluid mechanics description of the flow. In this approach, we use the Darcy law in a simplified two-dimensional Hele Shaw cell. We consider a blob of oil (with a volumetric mass ρ_o and a viscosity μ_o) immersed in a lighter fluid (volumetric mass ρ_w, viscosity μ_w). In the fracture, for a blob of oil of vertical height h, the superficial oil velocity is (Catalan et al. 1992):

$$q = \frac{k}{\mu_o h}((\rho_w - \rho_o)gh - P_c) \tag{2}$$

In this equation, the capillary pressure P_c is an opposite force to the oil migration, while the oil–water density difference is the driving force. It is important to note that the capillary pressure effect is negligible compared with gravitational effect when the height of oil h is large (or if there is a very high density difference between ρ_w and ρ_o).

The width W of the finger can be evaluated as proposed in reference (Nicholl and Glass 2005), arguing that the development of a finger begins from a flat interface to a rounded tip, with a tip radius $h = W/2$. Substituting this relation in Eq. 2 gives the approximate width of the finger,

$$W = \frac{2P_c}{(\rho_w - \rho_o)g - \frac{q\mu_o}{k}} \tag{3}$$

The estimation of W requires the knowledge of the mean value of P_c (which is a time and space dependant parameter). However, P_c can be simply bounded by two limit values (Glass

et al. 1998). For a capillary pressure controlled by the aperture of the fracture (capillary fingering model), P_c reaches the highest value, $P_c \approx \gamma/\bar{b}$, and it gives the order of magnitude of the largest value of the finger width:

$$W_{CP} = \frac{2\bar{b}}{Bo - Ca} \tag{4}$$

If the capillary pressure is controlled by the oil–water interface curvature in the plane of the fracture (Saffman and Taylor 1958) (Hele Shaw model), the capillary pressure is the lowest, $P_c \approx \gamma/(W/2)$. The substitution of this value in Eq. 3 gives the minimum bound for the finger width:

$$W_{HS} = \frac{2\bar{b}}{(Bo - Ca)^{1/2}} \tag{5}$$

Equations 3 and 4 are expressed with the two dimensionless parameters Bo and Ca, whereas the critical velocity (Eq. 1) depends on the modified parameter Ca'. Happily, for an oil–water displacement, these two numbers Ca and Ca' are quite close: in our experiments; their relative difference is around 10%, and in a few cases reaches 20%. This difference is negligible in logarithmic coordinates. Therefore, in the following, we will neglect the difference between Ca and Ca' It is interesting to note that Eq. 5 is nearly similar to the Safman–Taylor calculations, where the finger width is obtained through the linear stability analysis of transverse disturbances of wave length λ_c. The minimal wave length of unstable mode is (Saffman and Taylor 1958) $\lambda_c = 2\pi\bar{b}\frac{1}{(Bo-Ca')^{1/2}}$. The similarity with Eq. 5 enhances the coherence of the theoretical approach based on a strong assumption (Eq. 3). This result is also similar to the results presented in Nicholl and Glass (2005), but is rewritten here with two conventional dimensionless terms Ca and Bo.

The observed mean finger widths are plotted versus the Bond number, for three capillary numbers, corresponding to the three different injection velocities (Fig. 5a). The width W is measured on the pictures of Fig. 4, at the percolation threshold, and is averaged in the 25% top domain of the fracture. The mean finger width obtained in our experiment is compared with the lower prediction (Eq. 5). The theoretical curve has an interesting behaviour: the width of the finger decreases with the Bond number, because a higher density contrast enhances the vertical oil buoyancy and the instability. If the Bond number decreases, there is a stabilisation of the interface; the width of the finger increases and becomes infinite when Bo reaches Ca (or Ca', i.e. when q reaches q_c). When $Bo < Ca$, then $q < q_c$; the interface is stable and the model (Eqs. 4 and 5) cannot be applied ($W = l$). The theoretical higher bound (Eq. 4) field is not plotted on the figure, because W_{CP} gives values one or two orders of magnitude above the experimental ones. This emphasises that, in our experiments, the assumption of a capillary pressure controlled by the aperture is not pertinent to determine the width of the finger. For the two lowest capillary number experiments ($Ca = 1.77E-4$ and $Ca = 8.87E-4$), the theoretical predictions of Eq. 5 match relatively well the experimental results. The agreement is not perfect but a perfect fit cannot be expected because of the numerous assumptions made to obtain Eq. 5. Notice that Eq. 5 under-predicts the width of the string, while λ_c (the Saffman-Taylor result, not plotted on the Fig. 5a) slightly over-predicts the experimental results; but the order of magnitude is correct for both equations. Moreover, previous studies of gravitational fingering (for water–air top to bottom displacement) shows that an ideal quantitative description of the finger width is complex, particularly due to the large variability of the experimental results (Nicholl and Glass 2005; Nicholl et al. 1994; Mogensen and Stenby 1998). If we focus on the experiments at the highest capillary number, the theoretical width values are more underestimated. This result can be easily explained

arguing that the capillary pressure depends in fact on the flow velocity. In many studies of immiscible displacement in porous media (Annaka and Hanayama 2005; Weitz et al. 1987) or fracture (DiCarlo and Blunt 2000; Nicholl and Glass 2005), it was found that the capillary pressure increases with the fluid velocity (i.e. the capillary number). Following these previous studies, we use an empirical relation with an effective surface tension (which is proportional to the capillary pressure) expressed versus the capillary number, $\gamma_{\text{eff}} = \gamma(1 + \psi\ Ca^n)$. This estimation of P_c dependence on fluid velocity contains two adjustable parameters, Ψ and n. They are obtained with a non-linear regression analysis to have the best agreement between W and Bo (we find $\psi = 12$ and $n = 0.3$). Figure 5b shows that the agreement is satisfactory. However, the result obtained in Fig. 5a is also satisfactory (except at high capillary number) because a correct order of magnitude is obtained with the theory (Eq. 5). This indicates that the capillary pressure is controlled by the interface curvature in the plane of the fracture. This result was already noticed in numerous studies of immiscible fluids displacement in a Hele Shaw cell (Bensimon et al. 1986; Park et al. 1984; Zhang et al. 1998). We have seen, in the aperture field measurement section, that the correlation length of the aperture is of the same order of magnitude as the mean aperture. Therefore, the condition required to obtain a capillary regime displacement (i.e. $\bar{b} \ll \lambda$) is probably more complex as it was already suggested Glass et al. (1998).

4.4 Finger Tip Velocity

Equation 2 allows to analyse the finger tip velocity. It is easily measured from the pictures of Fig. 3 sampled over a shorter time interval. In all cases, the experimental tip velocity rapidly reaches a constant value. This velocity can also be theoretically estimated. Eq. 2 shows that the superficial velocity reaches the asymptotic value $k(\rho_w - \rho_o)g/\mu_o \approx q_c$ at large h. Therefore, it could be inferred that the finger tip moves with a velocity equal to the critical velocity threshold q_c. However, there is a very bad experimental agreement between the measured velocity and q_c. The reason is that q_c is a superficial velocity that depends on the width of the finger. It is convenient to calculate the velocity from a simple mass conservation law:

$$q_{tip} = \frac{Q}{bW_{HS}} \tag{6}$$

The theoretical velocity obtained from Eq. 6 is compared to our experimental measurements in Fig. 6. As the relation between the front width and the Bond number gives a reasonable agreement (Fig. 5b), we also have a satisfactory agreement between the finger tip velocity (Eq. 6) and the Bond number. The theory gives once again a good order of magnitude with quite small differences. A more detailed analysis is necessary to identify the reasons of these discrepancies.

The velocity of the finger as estimated in Eq. 6 assumes that a fully oil saturated and rectangular finger (of width W and thickness b) invades the cell. Actually, the finger has a geometrical tortuosity τ, and due to wetting effect, the thickness of the finger is not equal to the mean thickness of the fracture $\bar{b}$. The tortuosity effect diminishes the finger velocity, while a lower finger thickness increases the finger velocity. At this stage, a theoretical description of the finger velocity would require a better knowledge of the finger geometry, and of the oil velocity field within the finger. Also, the permeability of the fracture was assumed constant and equal to the permeability of a planar fracture, whereas other authors have used the concept of relative permeability (Catalan et al. 1992). An analysis of the finger velocity was proposed (Zhang and Smith 2001), introducing the concept of a mobile and immobile zone

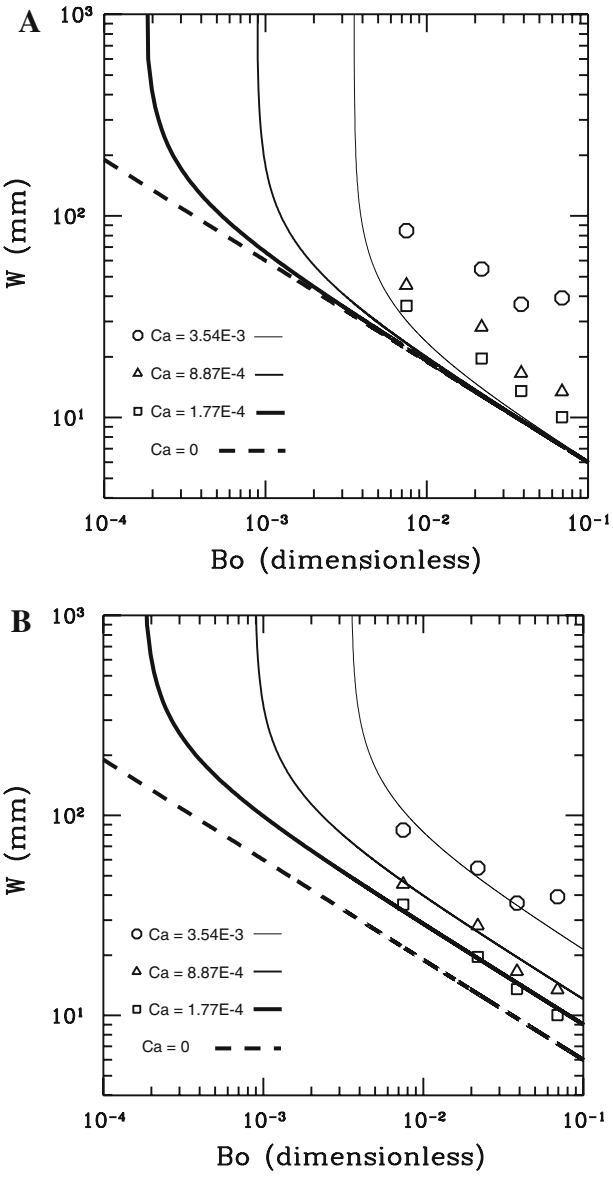

Fig. 5 **a** The transversal width of the oil finger W is plotted versus the dimensionless Bond number and for three flow rates (which correspond to three different capillary numbers): at 100 cm^3/h ($Ca = 3.54E-3$, *circle*), 25 cm^3/h ($Ca = 8.87E-4$, *triangle*) and 5 cm^3/h ($Ca = 1.77E-4$, *square*). The 4 lines of the figure are a representation of Eq. 5, giving the theoretical width of the string versus the Bond number and the capillary number. **b** This is the same as Fig. 5a, but the theoretical lines take into account the velocity dependance of the capillary pressure, using an effective surface tension $\gamma_{\text{eff}} = \gamma(1 + \psi Ca^n)$

in the finger. The result takes into account the finger tortuosity τ, the saturation within the finger θ, the relative permeability of the media k_r, and reads:

$$q_{tip2} = \frac{k_r(\rho_w - \rho_o)g\beta^2}{\mu_o \tau \theta} \tag{7}$$

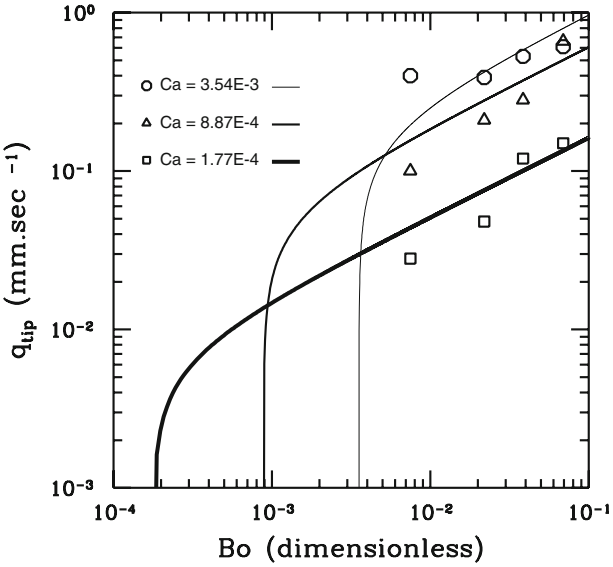

Fig. 6 The tip velocity is plotted versus the Bond number for three flow rates at 100 cm^3/h ($Ca = 3.54E-3$, *circle*), 25 cm^3/h ($Ca = 8.87E-4$, *triangle*) and 5 cm^3/h ($Ca = 1.77E-4$, *square*). The reasons for the discrepancy between the theory (Eq. 6) and experimental results are discussed in the text

The resulting formula is quite complicated to use, because various parameters act simultaneously with opposite effects on the velocity. In particular, the parameter β, which is the ratio of the mobile core to the whole finger, is difficult to estimate. Eq. 7 can however improve the interpretation of our results, provided that we define a relative permeability and the size of a conceptual finger with a mobile and immobile zone.

5 Phase Diagram for Vertical Oil Migration Pattern

Assimilating Ca and Ca', Eq. 1 shows that the flow is unstable when $Ca < Bo$, and is stable when $Ca > Bo$. In a log-log $Ca - Bo$ diagram (Fig. 7), the line of equation $Ca = Bo$ divides the diagram in a stable domain (above the line of equation $Ca = Bo$) and unstable zone (below the line of equation $Ca = Bo$). However, the stability condition obtained with Eq. 1 must be corrected as a consequence of the stability analysis, which predicts the width of the finger (Eq. 5, if we assume that P_c is $\gamma/(W/2)$). The width of the finger must be smaller than the width l of the cell ($W_{HS} < l$): it means that the condition $Ca < Bo - 4\frac{\tilde{b}^2}{l^2}$ has to be verified to permit the fingering growth. If we plot the line of equation $Ca = Bo - 4\frac{\tilde{b}^2}{l^2}$, then all the points above this equation are in a stable domain (coloured in dark grey), while all the points below the curve are in an unstable domain.

The experimental data are plotted on the stability diagram of Fig. 7. They show that the range of parameters explored by the present experiments is entirely in the unstable domain. Further experiments exploring the stable domain (e.g. with a smaller Bond number) would require a larger cell, because the width of the fingers increases if the Bond number decreases. Moreover, near the stability threshold, the width of the finger is expected to increase drastically, and the measurement of the velocity threshold may be blurred by the aperture heterogeneity of the fracture, whereas Eq. 1 that gives the critical velocity is only valid for a plane

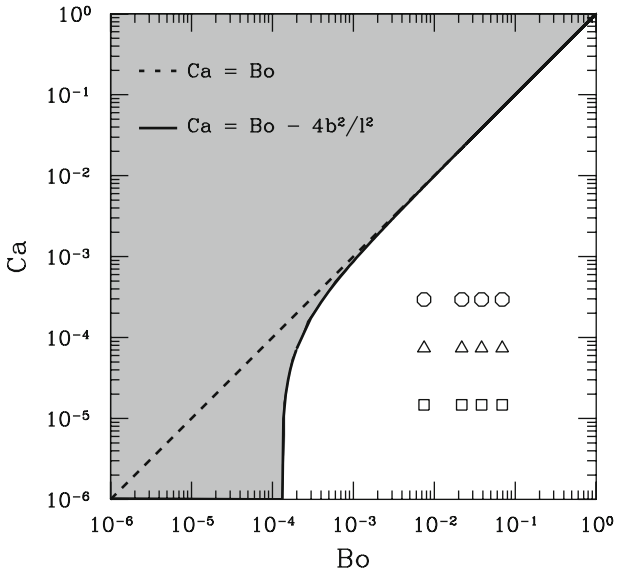

Fig. 7 Phase diagram for vertical and upward migration of a blob of oil of length h displacing a denser liquid in a planar fracture of aperture $\bar{b}$. The capillary number is plotted versus the Bond number. The dashed line $Ca = Bo$ divides the curve into a stable (*upper*) part and an unstable (*lower*) part. Taking into account the width of the fingering instability, the dashed line of equation $Ca = Bo$ is corrected by the full line ($Ca = Bo - 4\frac{\bar{b}^2}{l^2}$). All the experiments plotted as dots lie in the unstable domain

fracture. This is beyond the scope of this paper where the main goal is to study the instability patterns (length and tip of the finger, etc...).

6 Conclusion

The vertical oil migration in a transparent and rough fracture containing a wetting and denser fluid has been studied experimentally under the combined effects of gravity, viscous and capillary forces. The aperture of the fracture and the oil saturation has been measured using a transmission light technique.

Results have been described quantitatively using two conventional dimensionless numbers, the capillary number (Ca) and the Bond number (Bo). According to these two parameters, the oil dynamic pattern is classified into four distinct domains: piston-like displacement with trapping (high Ca and low Bo number), random cluster with tortuous finger (high Ca number and intermediate Bo number), single and tortuous finger (low Ca number and intermediate Bo number) and single and tortuous finger with fragmentation (low Ca number and high Bo number).

The critical velocity below which the flow is unstable and produces a gravitational finger is calculated versus the dimensionless parameters Ca and Bo. The width and velocity of the finger are also calculated versus Ca and Bo. Two solutions are obtained for the width and the velocity, depending on the assumption made on the capillary pressure. In a fracture, the capillary pressure is bounded by two limits depending on the radii of curvature of the oil–water interface: the first radius of curvature lies in the plane of the fracture, and the second one is perpendicular to the plane of the fracture. Our results support a capillary pressure where the controlling radius of curvature is in the plane of the fracture, the second one being unim-

portant. This assumption gives a reasonable agreement between the theory and experimental measurements of the width (and the velocity) of the finger, but there exists a small deviation between the experiment and theory. The discrepancy can be explained by several concepts: the dependence of capillary pressure on velocity, the tortuosity of the finger, the oil complex velocity field into the finger and the unknown thickness of the finger into the gap of the cell. All these parameters can act on the velocity and/or the width of the finger. For this reason, it is not possible to completely explain the difference between the theory and the experiments.

Nevertheless, the hypothesis and the simplified approach presented here provide an acceptable quantitative description of our experimental results, and they offer some perspectives and suggestions for further studies: our results concern a fracture with a low degree of heterogeneity; it would be very interesting to study upward oil migration when the correlation length of the aperture is much more smaller than the mean aperture, with a capillary pressure mainly controlled by the aperture heterogeneity. The injection of oil through a single point gives rise to a single finger; it will be interesting to test a multiple points injection experiment with an imposed flow rate or in the absence of flow rate (pure buoyancy displacement). It would also be interesting to use a more sophisticated device to measure the oil velocity field and the finger thickness during the displacement.

References

Amundsen, H., Wagner, G., Oxaal, U., Meakin, P., Feder, J., Jossang, T.: Slow two-phase flow in artificial fractures: experiments and simulations. Water Resour. Res. **35**(9), 2619–2626 (1999)

Annaka, T., Hanayama, S.: Dynamic water-entry pressure for initially dry glass beads and sea sand. Vadose Zone J. **4**(1), 127–133 (2005)

Bensimon, D., Kadanoff, L.P., Liang, S., Shraiman, B.I., Tang, C.: Viscous flows in two dimensions. Rev. Mod. Phys. **58**(4), 977–999 (1986)

Bo, Z., Loggia, D., Xiarong, L., Vasseur, G., Ping, H.: Numerical studies of gravity destabilized percolation in 2D porous media. Eur. Phys. J. B **50**, 631–637 (2006)

Catalan, L., Xiaowen, F., Chatzis, I., Dullien, F.A.L.: An experimental study of secondary oil migration. AAPG Bull. **76**(5), 638–650 (1992)

Chuoke, R.L., van Meurs, P., van der Poel, C.: The instability of slow, immiscible, viscous liquid–liquid displacements in permeable media. Pet. Trans. AIME **216**, 188–194 (1959)

Detwiler, R.L., Pringle, S.E., Glass, R.J.: Measurement of fracture aperture fields using transmitted light: An evaluation of measurement errors and their influence on simulations of flow and transport through a single fracture. Water Resour. Res. **35**, 2605–2618 (1999)

DiCarlo, D.A., Blunt, M.J.: Determination of finger shape using the dynamic capillary pressure. Water Resour. Res. **36**(9), 2781–2785 (2000)

Ewing, R.P., Berkowitz, B.: A generalized growth model for simulating initial migration of dense nonaqueous phase liquids. Water Resour. Res. **34**(4), 611–622 (1998)

Glass, R.J., Yarrington, L.: Simulation of gravity fingering in porous media using a modified invasion percolation model. Geoderma **70**, 231–252 (1996)

Glass, R.J., Nicholl, M.J., Yarrington, L.: A modified invasion percolation model for lowcapillary number immiscible displacements in horizontal rough-walled fractures: influence of local in-plane curvature. Water Resour. Res. **34**(12), 3215–3234 (1998)

Loggia, D., Rakotomalala, N., Salin, D., Yortsos, Y.C.: Evidence of new instability thresholds in miscible displacements in porous media. Eur. Phys. Lett. **32**, 633–638 (1995)

Loggia, D., Gouze, P., Greswell, R., Parker, D.J.: Investigation of the geometrical dispersion regime in a single fracture using positron emission projection imaging. Trans. Porous Media **55**, 1–20 (2004)

Mogensen, K., Stenby, E.H.: A dynamic two-phase pore-scale model of imbibition. Trans. Porous Media **32**, 299–327 (1998)

Nicholl, M.J., Glass, R.J.: Infiltration into an analog fracture: Experimental observations of gravity-driven fingering. Vadose Zone J. **4**, 1123–1151 (2005)

Nicholl, M.J., Glass, R.J., Wheatcraft, S.W.: Gravity-driven infiltration instability in initially dry non-horizontal fractures. Water Resour. Res. **30**(9), 2533–2546 (1994)

Nicholl, M.J., Rajaram, H., Glass, R.J.: Factors controlling satiated relative permeability in a partially-saturated horizontal fracture. Geophys. Res. Lett. **27**(3), 393–396 (2000)
Park, C.-W., Gorrell, S., Homsy, G.M.: Two-phase displacement in Hele-Shaw cells: experiments on viscously driven instabilities. J. Fluid Mech. **141**, 275–287 (1984)
Peters, E.J., Flock, D.L.: The onset of instability during two-phase immiscible displacement in porous media. Soc. Pet. Eng. **8371**, 249–258 (1981)
Riaz, A., Tchelepi, H.A.: Linear stability analysis of immiscible two-phase flow in porous media with capillary dispersion and density variation. Phys. Fluids **16**(12), 4727–4737 (2004)
Saffman, P.G., Taylor, G.L.: The penetration of a fluid into a porous medium or Hele-Shaw cell containing a more viscous liquid. In: Proc. R. Soc. Lond. **A245**, 312–331 (1958)
Weitz, D.A., Stokes, J.P., Ball, R.C., Kushnick, A.P.: Dynamic capillary pressure in porous media: origin of the viscous-fingering length scale. Phys. Rev. Lett. **59**(26), 2967–2970 (1987)
Wilkinson, D.: Percolation model of immiscible displacement in the presence of buoyancy forces. Phys. Rev. A **30**, 520–531 (1984)
Zhang, Z.F., Smith, J.E.: The velocity of DNAPL fingering in water-saturated porous media: laboratory experiments and a mobileimmobilezone model. J. Contam. Hydrol. **49**(3–4), 335–353 (2001)
Zhang, S.-Z., Louis, E., Pla, O., Guinea, F.: Linear stability analysis of the Hele-Shaw cell with lifting plates. Eur. Phys. J. B **1**, 123–127 (1998)